Asymptotic analysis of a Hiemenz flow in a low-porosity medium with phase change

Max A. E. Kokubun and Fernando F. Fachini

Journal of Fluid Mechanics / Volume 698 / May 2012, pp 185 - 210
DOI: 10.1017/jfm.2012.75, Published online: 30 March 2012

J. Fluid Mech. (2012), *vol.* 698, *pp.* 185–210.
doi:10.1017/jfm.2012.75

Asymptotic analysis of a Hiemenz flow in a low-porosity medium with phase change

Max A. E. Kokubun† and Fernando F. Fachini

Laboratório de Combustão e Propulsão, Instituto Nacional de Pesquisas Espaciais, 12630-000 Cachoeira Paulista, SP, Brazil

(Received 30 May 2011; revised 26 October 2011; accepted 3 February 2012; first published online 30 March 2012)

In the present work, the features of liquid evaporation inside a low-porosity medium subjected to an impinging stream of hot gas is investigated analytically. The flow is analysed for a non-Darcy model, in which viscous and convective terms are considered in the Darcy pressure equation. A low-volatility liquid is considered, so that a low-vaporization regime is established. The rates of heat transfer between gas and solid and between liquid and solid are assumed to be high. Owing to differences between phase properties, in the system under study, different physical processes occur at different length scales. Using asymptotic expansions, expressions for the three phases that occur in this problem are obtained, in each of their length scales. The results predict that high injection temperatures are needed for phase change to occur, as a result of the low volatility of the liquid. Likewise, the enhancement of the vaporization rate due to heat conduction in the porous medium is quantified. The Hiemenz flow pressure term is modified to incorporate the effect of the porous medium, which is necessary for a solution to be found.

Key words: condensation/evaporation, convection in porous media, porous media

1. Introduction

In the last decades, use of porous-medium-based technologies has led to the design of more effective heat exchangers. Indeed, improvements of interphase heat transfer rates are reported when using porous materials, as a result of the increase of the contact area between fluid and solid (Konstatinou *et al.* 1997; Alkam & Al-Nimr 1999; Furberg *et al.* 2009; Yang & Hwang 2009; Dyga & Placzek 2010). This increase leads to an enhancement in the thermal conductivity of the system. Modulated porous-layer coatings (coatings designed with periodic variations in the layer thickness) have been studied, showing a significant enhancement of the pool boiling critical heat flux (Liter & Kaviany 2001).

Studies concerning phase change in porous media are extensively found in the literature due to the vast amount of potential applications (Yortsos & Stubos 2001). Drying processes (Daurelle, Topin & Occelli 1998), geothermal systems (Woods 1999) and nuclear safety issues are some examples of these system. The presence of intrinsically coupled physical processes offers a fertile ground for fundamental scientific research. Owing to viscosity, boundary layers occur on pore walls, with

† Email address for correspondence: max@lcp.inpe.br

length scaling with the square of the medium permeability. Furthermore, the tortuous channels in the porous medium result in additional resistance against the flow. If the system is not thermally at equilibrium, interphase heat exchange will also result in a coupled heat transfer problem between the two phases, which will depend upon the thermo-physical properties of the porous medium, resulting in a rather complex set of coupled governing equations.

The evaporation of a thin film of liquid water within a heated porous bed subjected to a stagnation-point flow was studied analytically (Zhao 1999). Local thermal equilibrium was considered, and the focus was on the influence of the parameters on heat and mass transfer. The obtained results are of significance for the design of indirect evaporative air cooler systems.

Local thermal non-equilibrium in a three-phase problem was studied by Duval, Fichot & Quintard (2004), who, using the volume-averaging method, derived a three-temperature macroscopic model considering local thermal non-equilibrium between the three phases. They obtained a closed-form expression for the evaporation rate at the macroscopic level, that depends upon macroscopic temperatures and effective properties. Under the quasi-steady and quasi-static assumptions at the closure level, the authors obtained a macroscopic model consisting of a three-equation model involving relevant non-equilibrium terms in which the saturation temperature appeared explicitly. Their results for the evolution of both macroscopic temperatures and liquid volume fraction were compared with numerical results in the case of a heating problem and of a temperature relaxation problem.

Boiling in a saturated porous medium was analysed by Ramesh & Torrance (1993) by considering heat supply from below and cooling from above. Using numerical simulation, they analysed the possible flow regimes in the presence of a moving liquid/two-phase interface. The authors conducted a parametric study considering the effect of the liquid-phase Rayleigh number and the dimensionless bottom heat flux. From their results, they identified three different regimes: conduction dominated for low Rayleigh number, convection dominated for intermediate Rayleigh number and oscillatory convection for high Rayleigh number. In the convection-dominated regime, as the dimensionless bottom heat flux increases, transition to multiple cell patterns was observed. The stability of these solutions in the presence of perturbations was also analysed. The study considered a fixed interphase heat exchange, expressed as a heat loss parameter.

The effect of local thermal non-equilibrium on the infiltration of a hot fluid into a cold porous medium was studied by Rees, Bassom & Siddheshwar (2008). In order to study this flow configuration, the moving thermal front resulting from thermal non-equilibrium was analysed. From dimensional analysis and numerical simulations, the different ways in which the temperature fields evolve in time were discussed. It was found that the thickness of the thermal front is a function of the dimensionless interphase heat transfer parameter, of the porosity-modified conductivity ratio and of the diffusivity ratio. This implies that local thermal equilibrium is not equivalent to a single equation formulation of the energy equation. Their results for a long time analysis showed that local thermal equilibrium is achieved in the long limit, but that the solution differs from the solution obtained from a one-equation model. They also observed the formation of a shock wave when the velocity of the infiltrating fluid was sufficiently large.

There are many studies in the open literature concerning natural evaporation, especially on analysis of the drying process of porous media. That problem is concerned with applications in areas such as wood, paper and the textile industry.

Il'ichev *et al.* (2008) studied gravitational instability of the salinity profile during the evaporation of saline groundwater. The stability analysis concluded that the most significant effect controlling the stability is the permeability of the soil. The effects of the different characteristic length scales in the problem of evaporative drying of a porous medium was analysed by Lehmann, Assouline & Or (2008). By comparing the roles of gravity, surface tension and viscous dissipation forces, they deduced the characteristic length for the maximum hydraulically connected film region between the drying front and the surface. These characteristic lengths depend upon the range of sizes between the smallest and largest pores within the film region. For media with large pores sizes, the characteristic length is dominated by gravity and capillarity, while viscous dissipation is negligible. For fine-textured media, with small pores sizes, viscous dissipation may limit the maximum hydraulically connected distance between the drying front and the evaporating surface. The authors also conducted experiments with two types of sand in order to determine the characteristic lengths and the extent of the film region.

Vapour extraction from a water-saturated porous reservoir (Woods & Fitzgerald 1993; Tsypkin & Woods 2004), condensing flow of steam (Bergins, Crone & Strauss 2005), motion of aqueous saline solution through a low-permeability fracture (Tsypkin & Woods 2005), gas extraction from multilayered rocks (Farcas & Woods 2007) represent examples of geothermal applications of phase change in porous media.

However, the problem of heat supplied to a liquid by a hot impinging gas in a porous medium does not appears to have been subjected to analysis so far. This situation will arise for instance in the steam injection process for thermal oil recovery (Arnold 1989; Jabbour *et al.* 1996; Prats 2003). When a well contains heavy oil, its recovery may be achieved by means of heat addition in the reservoir, increasing its temperature and lowering the viscosity of the oil, hence increasing its mobility. In that application, a high initial (injection) temperature of the steam will be required. Another thermal recovery method for heavy oils which also presents evaporation of a low-volatility liquid is the *in situ* combustion process (Castanier & Brigham 2003). In this method, part of the heavy oil is burned in the well in order to lower the petroleum viscosity. However, before the combustion process takes place, the part of the heavy oil to be burned must evaporate, since it is the heavy oil vapour mixed with the injected oxidant that is consumed in the exothermic reaction. As in the steam injection process, the oxidant must be injected at high temperatures. Owing to the economic and strategic aspect of the thermal oil recovery methods, the study of such a problem is extremely relevant.

Focusing upon that system, the present work analyses the impinging jet over a pool of a low-volatility liquid present in a low-porosity medium and subject to phase change, for high rates of interphase heat transfer. The occurrence of physical processes in different length scales runs out to be crucial in this problem. The high interphase heat transfer assumption leads to thermal equilibrium between phases (gas–solid and liquid–solid) in most of the domain, where the one-equation approach is valid. However, close to the gas–liquid interface, thermal non-equilibrium is observed between phases. As a result, in a small region near the interface, the two-equation model (for the gas–solid region and for the liquid–solid region) must be used. The non-equilibrium zone is analysed using expansions similar to those employed in the boundary-layer analysis from energy and mass conservation at the gas–liquid interface, the formulation determines the relevant unknown parameters (vaporization rate, solid phase temperature at the interface and vapour mass fraction at the interface). The

Dimensional variables		v	Vertical velocity
c_l	Liquid-phase specific heat	x	Horizontal spatial coordinate
c_p	Gas-phase specific heat	y	Mass fraction
$\bar{D}$	Mass diffusion coefficient	z	Vertical spatial coordinate
h	Heat transfer coefficient		(Liquid–solid region)
K	Medium permeability	$\tilde{z}$	Vertical spatial coordinate
L	Latent heat of vaporization		(Boiling zone)
ls	Length scale		
$\bar{\dot{m}}$	Vaporization rate	*Greek symbols*	
$\bar{p}$	Pressure	α	Thermal diffusivity
T	Temperature	β	Unitary order
$\bar{u}$	Horizontal velocity		Permeability parameter
$\bar{v}$	Vertical velocity	$\gamma \equiv (1-\varepsilon)/\varepsilon$	Porosity parameter
$\bar{x}$	Horizontal spatial component	$\Gamma \equiv \lambda_s/\lambda_g$	Thermal conductivities ratio
$\bar{z}$	Vertical spatial component	ε	Medium porosity
		η	Vertical spatial coordinate
Dimensionless variables		$\hat{\eta}$	Vertical spatial coordinate
a	Strain rate		(Intermediary zone)
f	Vertical momentum	$\tilde{\eta}$	Vertical spatial coordinate
$\hat{f}$	Vertical momentum		(Inner zone)
	(Intermediary zone)	θ	Dimensionless temperature
$\tilde{f}$	Vertical momentum	κ	Modified Darcy number
	(Inner zone)	λ	Thermal conductivity
$J \equiv \lambda_l/\lambda_s$	Thermal conductivities ratio	μ	Dynamic viscosity
l	Latent heat of vaporization	ν	Kinematic viscosity
$\tilde{l}$	Unitary order	ρ	Mass density
	Latent heat of vaporization	ϱ	Dimensionless density
Le	Lewis number		
$\dot{m}$	Vaporization rate	*Subscripts*	
M	Modified vaporization rate	b, B	Boiling
n	Unitary order	F	Vapour phase
	Heat transfer parameter	g	Gas phase
N	Heat transfer parameter	l	Liquid phase
p	Pressure	s	Solid phase
Pe	Peclet number	st	Stagnation
Pr	Prandtl number	0	Interface conditions
u	Horizontal velocity	$-\infty$	Reservoir conditions
U	Boundary layer	∞	Injection conditions
	Horizontal velocity		

TABLE 1. Nomenclature.

appearance of a large parameter, namely the ratio between solid and gas phases thermal conductivities, in the dimensionless conservation equations allows to seek solutions by means of perturbation theory (Van Dyke 1964; Kevorkian & Cole 1981; Nayfeh 1981). Even though analytical analyses do not provide detailed information that could be applied directly, such as that obtained in a numerical investigation, deep qualitative results and, consequently, a high understanding of the physical aspects of the problem, are achieved by means of theoretical analyses.

Results predict the need of high-temperature injection for the evaporation process to occur. Phase change enhancement due to introduction of the porous medium in the free system, as a result of heat conduction in the solid matrix, is quantified.

2. Length scales

The most significant originality of the current work consists in the identification of different length scales that characterize the different physical processes, allowing for an asymptotic solution.

Four distinct boundary layers can be identified in the system under consideration. The first is a macroscopic boundary layer, similar to the classical boundary layer in viscous flows. A pore-level boundary layer, defined as the Darcy boundary layer, due to viscous forces on the pore walls, is of the order of the square of the medium permeability. The last two layers are thermal in nature; their thickness is associated with the non-equilibrium zones, respectively, between gas–solid and liquid–solid.

The characteristic length scale considered in this work is the scale characterizing heat conduction in the solid phase (solid-thermal-conductivity-based Péclet number equal to one, $Pe_s = 1$), given by $ls_s \equiv \lambda_s/(\rho_\infty c_p \bar{v}_\infty)$ (Pereira, Oliveira & Fachini 2009, 2010; Kokubun & Fachini 2011).

Only in a region of the order of the gas-phase diffusivity, given by $ls_g \equiv \lambda_g/(\rho_\infty c_p \bar{v}_\infty)$ is non-equilibrium between gas and solid observed. The ratio between these two length scales is given by $\Gamma \equiv ls_s/ls_g \gg 1$.

The magnitudes of the gas and liquid dimensionless heat transfer parameters are assumed to be $N_g = O(\Gamma)$ and $N_l = O(\Gamma^2)$, respectively. This situation corresponds to injection of the hot gaseous stream at low velocity (from the definition of the dimensionless heat transfer parameters), which is typical of steam injection into petroleum wells.

Below the gas–liquid interface, most of the liquid–solid system is at thermal equilibrium. The temperature of the liquid–solid system increases as a result of the heat flux incoming from the gas–solid region. However, in a small region just below the gas–liquid interface, the temperature of the liquid no longer increases, as its boiling temperature has been reached, and almost all of the heat delivered contributes to phase change. The solid matrix, on the other hand, does not have such a constraint, and its temperature continues to increase as a result of conductive heat transport in the solid phase, from the gas–solid region. Thus, in this small boiling (phase change) zone, liquid and solid are not in thermal equilibrium. This non-equilibrium is the main responsible for providing the necessary heat to the liquid to undergo phase change, as will be seen.

The volatility of the liquid is considered to be low, resulting in a low vaporization regime. Vapour is only observed close to the gas–liquid interface. Figure 1 presents a schematic representation of the current problem, with the inner regions (viscous and boiling) shown in the detail picture.

3. Mathematical formulation

The geometry under consideration consists of a stream of hot gas impinging over the surface of a liquid pool. The domain is divided into two regions: a region in which the solid matrix is filled by gas (gas–solid region), and a region in which the solid matrix is filled by liquid (liquid–solid region). The geometry is two-dimensional, with two spatial coordinates: $\bar{z}$ is normal to the liquid surface and $\bar{x}$ is tangential to the liquid surface, as shown in figure 1.

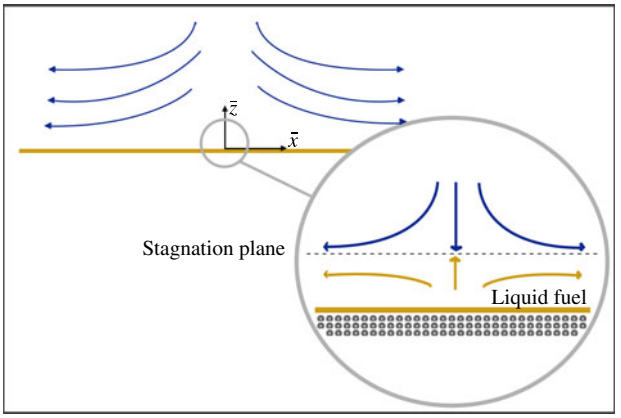

FIGURE 1. Schematic representation of the problem.

A boundary-layer approximation leads to the variables depending only upon the $\bar{z}$ coordinate. The thermal expansion of the gas is assumed to be negligibly small, so that an equation of state is not required and the temperature field does not influence the velocity field. The thermo-physical properties of the impinging gas and of the vapour are assumed to be constant, as well as those of the solid matrix thermo-physical, and also the geometry.

For the gas–solid region, the stationary conservation equations are then given by (Kokubun & Fachini 2011)

$$\frac{\partial \bar{u}}{\partial \bar{x}} + \frac{\partial \bar{v}}{\partial \bar{z}} = 0, \tag{3.1}$$

$$\rho \bar{u} \frac{\partial \bar{u}}{\partial \bar{x}} + \rho \bar{v} \frac{\partial \bar{u}}{\partial \bar{z}} = -\varepsilon \frac{\partial \bar{p}}{\partial \bar{x}} + \mu \frac{\partial^2 \bar{u}}{\partial \bar{z}^2} - \varepsilon \mu \frac{\bar{u}}{K}, \tag{3.2}$$

$$\varepsilon \rho \bar{v} \frac{\mathrm{d}y_F}{\mathrm{d}\bar{z}} = \varepsilon \rho D_F \frac{\mathrm{d}^2 y_F}{\mathrm{d}\bar{z}^2}, \tag{3.3}$$

$$\varepsilon \rho \bar{v} c_p \frac{\mathrm{d}T_g}{\mathrm{d}\bar{z}} = \varepsilon \lambda_g \frac{\mathrm{d}^2 T_g}{\mathrm{d}\bar{z}^2} + h_g (T_s - T_g), \tag{3.4}$$

$$0 = (1 - \varepsilon) \lambda_s \frac{\mathrm{d}^2 T_s}{\mathrm{d}\bar{z}^2} - h_g (T_s - T_g). \tag{3.5}$$

Equation (3.2) considers viscous and convective terms in the Darcy equation in order to analyse their effects in the flow field. The boundary conditions far from the gas–liquid interface ($\bar{z} \to \infty$) are

$$\bar{v} = \bar{v}_\infty, \quad \bar{u} = \bar{x} \left. \frac{\mathrm{d}\bar{u}}{\mathrm{d}\bar{x}} \right|_\infty, \quad T_g = T_s = T_\infty, \tag{3.6}$$

and at the interface ($\bar{z} = 0$)

$$\bar{v} = \bar{v}_0, \quad T_g - T_{g0} = T_s - T_{s0} = 0, \quad y_F = y_{F0}, \tag{3.7}$$

in which y_{F0} is the vapour mass fraction at the interface. The interface divides liquid, at $\bar{z} = 0^-$, and vapour, at $\bar{z} = 0^+$. At the interface, liquid and vapour are in equilibrium at the boiling temperature, T_B, of the liquid, such that it will be considered that $T_{g0} = T_B$.

The velocity of the gas at the liquid surface, $\bar{v}_0$, is related with the vaporization rate, $\dot{\bar{m}}$, through

$$\rho.\bar{v}_{0^+} = \rho_l \cdot \bar{v}_{l0^-} = \dot{\bar{m}}, \tag{3.8}$$

and the velocities $\bar{v}_{0^+}$ ($\equiv\bar{v}_0$) and $\bar{v}_{l0^-}$ ($\equiv \bar{v}_{l0}$) represent the velocities of vapour and liquid at the interface; the subscripts $+$ and $-$ denote the gas side and liquid side of the liquid surface, respectively.

The thermo-physical properties of the liquid are assumed to be constant. With these considerations, the stationary conservation equations in the liquid–solid region are then given by

$$\rho_l \bar{v}_l = \dot{\bar{m}}, \tag{3.9}$$

$$\varepsilon\rho_l\bar{v}_l c_l \frac{\mathrm{d}T_l}{\mathrm{d}\bar{z}} = \varepsilon\lambda_l \frac{\mathrm{d}^2 T_l}{\mathrm{d}\bar{z}^2} + h_l(T_s - T_l), \tag{3.10}$$

$$0 = (1-\varepsilon)\lambda_s \frac{\mathrm{d}^2 T_s}{\mathrm{d}\bar{z}^2} - h_l(T_s - T_l). \tag{3.11}$$

The boundary conditions far below the interface ($\bar{z} \to -\infty$) are

$$T_l = T_s = T_{-\infty}, \quad \bar{v}_l = \bar{v}_{l-\infty}. \tag{3.12}$$

The injection velocity, $\bar{v}_{l-\infty}$, is such that the gas–liquid interface remains stationary at $\bar{z} = 0$.

At the gas–liquid interface, mass and energy conservation must be obeyed

$$\rho D_F \left.\frac{\partial y_F}{\partial \bar{z}}\right|_{\bar{z}=0} = -(1 - y_{F0})\rho\bar{v}_0, \tag{3.13a}$$

$$\varepsilon\lambda_g \left.\frac{\mathrm{d}T_g}{\mathrm{d}\bar{z}}\right|_{\bar{z}=0^+} = \rho\bar{v}_0 L + \varepsilon\lambda_l \left.\frac{\mathrm{d}T_l}{\mathrm{d}\bar{z}}\right|_{\bar{z}=-\bar{z}_b} - h_l \int_{-\bar{z}_b}^{0^-} (T_s - T_l)\,\mathrm{d}\bar{z}. \tag{3.13b}$$

The mass conservation condition at the interface, given by (3.13*a*), shows that the mass flux right above the liquid interface is resultant from the amount of liquid fuel vaporized below the interface. The integral term in (3.13*b*) is a consequence of the coexistence of liquid and vapour produced by the contact of the liquid on the hot porous wall. Owing to the expansion in the phase change process, the liquid is pushed to the region of the porous media with even higher temperature, which intensifies even more the vaporization. To model these processes in a simplified way, we admit the existence of a zone of thickness $\bar{z}_b$, just below the interface, in which the heat transfer from solid to liquid occurs at a constant liquid temperature. In this zone, phase change of the liquid occurs. Hence, the integral term in the right-hand side of (3.13*b*) accounts for the heat exchange between solid and liquid in the phase change (boiling) zone.

3.1. *Non-dimensional equations*

The non-dimensional variables are defined as $u \equiv \bar{u}/\bar{v}_\infty$, $v \equiv \bar{v}/\bar{v}_\infty$, $v_l \equiv \bar{v}_l/\bar{v}_\infty$, $\rho/\rho_\infty = 1$, $\varrho_l \equiv \rho_l/\rho_\infty$, $p \equiv \bar{p}/(\rho_\infty \bar{v}_\infty^2)$, $x \equiv \bar{x}/ls_s$, $z \equiv \bar{z}/ls_s$, $\theta_g \equiv T_g/T_\infty$, $\theta_s \equiv T_s/T_\infty$ and $\theta_l \equiv T_l/T_\infty$. The non-dimensional strain rate is defined as $a \equiv (ls_s/\bar{v}_\infty)\,\mathrm{d}\bar{u}/\mathrm{d}\bar{x}|_\infty$. Following Schilichting (1968), a modified variables change is performed in order to analyse the region near the stagnation point

$$u = axU(z), \quad v = -a^{1/2} f, \tag{3.14}$$

$$p_0 - p = \frac{1}{2} Pr\, a^2 \left(1 + \frac{1}{\kappa\Gamma}\right)\left[x^2 + \frac{2F(z)}{a}\right], \quad \eta = a^{1/2} z, \tag{3.15}$$

in which $Pr \equiv \nu/\alpha$ is the Prandtl number, $\Gamma \equiv \lambda_s/\lambda_g \gg 1$ and κ is the modified Darcy number based on the scale of the solid phase heat conduction, defined as $\kappa \equiv aK/ls_s^2 = (a/\Gamma^2)(K/ls_g^2)$. The pressure expression is based on the classical expression (Schilichting 1968) with an extra term, $1/(\kappa\Gamma)$, to consider the Darcy effect. As defined, the Hiemenz flow Darcy number, κ, also includes the effect of the flow strain rate, a, and it can also be expressed as

$$\kappa \equiv \frac{aK}{ls_s^2} = \frac{1}{\Gamma^2}\frac{aK}{ls_g^2} \equiv \frac{\kappa_g}{\Gamma^2} = \frac{1}{\Gamma^2}\left(\frac{aKPr^2}{\nu^2/\bar{v}_\infty^2}\right) \tag{3.16}$$

in which κ_g is the modified Darcy number based on the scale of the gas phase heat conduction. According to the assumed conditions in the present work, the modified Darcy number κ is very small, precisely $\kappa = O(\Gamma^{-2})$ (or $\kappa_g = O(1)$). Hence, the Darcy number, κ, is re-scaled as $1/(\kappa\Gamma) = \beta\Gamma$, in which β is a unitary order parameter that determines the type of porous medium.

In addition, it is considered that the non-dimensional gas and liquid volumetric surface convection heat coefficients are $N_g/a = n_g\Gamma$ and $N_l = n_l\Gamma^2$, in which n_g and n_l are unitary order parameters that collects information about the thermal interaction between solid and gas and between solid and liquid, respectively.

Performing the changes, (3.1)–(3.5) become

$$U = \frac{\mathrm{d}f}{\mathrm{d}\eta}, \tag{3.17}$$

$$\frac{Pr}{\Gamma}\frac{\mathrm{d}^3 f}{\mathrm{d}\eta^3} + f\frac{\mathrm{d}f^2}{\mathrm{d}\eta^2} - \left(\frac{\mathrm{d}f}{\mathrm{d}\eta}\right)^2 - \Gamma\varepsilon\beta Pr\frac{\mathrm{d}f}{\mathrm{d}\eta} = -\varepsilon Pr(1+\beta\Gamma), \tag{3.18}$$

$$\frac{1}{\Gamma}\frac{\mathrm{d}^2 y_F}{\mathrm{d}\eta^2} + Le_F f\frac{\mathrm{d}y_F}{\mathrm{d}\eta} = 0, \tag{3.19}$$

$$-\varepsilon f\frac{\mathrm{d}\theta_g}{\mathrm{d}\eta} = \frac{\varepsilon}{\Gamma}\frac{\mathrm{d}^2\theta_g}{\mathrm{d}\eta^2} + \Gamma n_g(\theta_s - \theta_g), \tag{3.20}$$

$$0 = (1-\varepsilon)\frac{\mathrm{d}^2\theta_g}{\mathrm{d}\eta^2} - \Gamma n_g(\theta_s - \theta_g), \tag{3.21}$$

in which, $Le_F \equiv \alpha_g/D_F$ is the vapour Lewis number.

The ratio $\Gamma^{-1} \equiv \lambda_g/\lambda_s$ determines the thickness of the macroscopic classical boundary layer, as it appears in the first term on the left-hand side of (3.18): the macroscopic viscous term. The non-dimensional parameter κ (the Darcy number) relates the medium permeability with the thermo-physical properties of gas and solid phases, and its magnitude determines the flow field. Its value is directly related to the boundary layer existent at the fluid–porous level of interaction ($K^{1/2}$ determines the thickness of the Darcy boundary layer). The thermal boundary layer is determined by the magnitude of the parameter N_g. The parameters κ and N_g are chosen in such a way that the three distinct boundary layers have the same thickness, Γ^{-1}.

A quick inspection on the magnitude order of the terms in (3.18) can be performed in order to analyse the effects of different permeability (porosity) media.

If a lower porosity (permeability) medium was considered, by using, for instance, $\kappa \sim \Gamma^{-3}$, the Darcy flow would be observed in the outer zone and practically in the whole inner zone. Therefore, the Darcy boundary layer would not have the same thickness of the thermal and viscous boundary layers. In this situation, the viscous effects of the porous medium internal area would establish the Darcy boundary layer

in a zone thinner than the inner zone (the Darcy boundary layer is of the order of $\kappa^{1/2}$ and, hence, in this case would be of the order of $\Gamma^{-3/2}$). On the other hand, if a higher porosity (permeability) medium was considered, by using, for instance, $\kappa \sim \Gamma^{-1}$, the flow in the outer zone would be dominated by the Darcy equation with the inertia terms. In this situation, the porous–fluid interaction would be minimized, and in the scale of Γ^{-1} the Darcy boundary layer would not be observed, since it would be of the order of $\Gamma^{-1/2}$. Hence, the choice of $\kappa \sim \Gamma^{-2}$ couples the three distinct boundary layers (Darcy, macroscopic viscous and thermal) in a region of the order of Γ^{-1} (inner zone).

The boundary conditions far from the interface ($\eta \to \infty$) are

$$\frac{\mathrm{d}f}{\mathrm{d}\eta} = U_\infty, \quad \theta_s = \theta_g = 1, \quad y_F = 0, \tag{3.22}$$

and at the interface ($\eta = 0$)

$$\frac{\mathrm{d}f}{\mathrm{d}\eta} = f - f(0) = 0, \quad \theta_s - \theta_{s0} = \theta_g - \theta_B = 0, \quad y_F = y_{F0}. \tag{3.23}$$

Recalling, the first condition $U = \mathrm{d}f/\mathrm{d}\eta = 0$ means no-slip flow on the liquid surface and the second one, as the others, corresponds to continuity of the properties through the surface. The exception is the mass fraction, because y_{F0} is the value of the mass fraction of the vapour at the gas side of the liquid surface, but at the liquid side of the surface $y_F = 1$.

Performing the variable changes given by (3.15) in (3.9)–(3.11), the following conservation equations for the liquid–solid region are obtained

$$\varrho_l v_l = \dot{m} \equiv \frac{\bar{\dot{m}}}{\rho_\infty \bar{v}_\infty}, \tag{3.24}$$

$$\varepsilon J \frac{\mathrm{d}^2\theta_l}{\mathrm{d}z^2} - \varepsilon M \frac{\mathrm{d}\theta_l}{\mathrm{d}z} = -\Gamma^2 n_l(\theta_s - \theta_l), \tag{3.25}$$

$$(1-\varepsilon)\frac{\mathrm{d}^2\theta_s}{\mathrm{d}z^2} = \Gamma^2 n_l(\theta_s - \theta_l), \tag{3.26}$$

in which $M \equiv \dot{m}(c_l/c_p)$ and $J \equiv \lambda_l/\lambda_s$. The boundary conditions far below the interface ($z \to -\infty$), characterized by the thermal equilibrium between the phases, are

$$\theta_l = \theta_s = \theta_{-\infty}. \tag{3.27}$$

Non-dimensional mass and energy conservation at the interface are given by

$$\frac{1}{\Gamma}\frac{1}{Le_F}\frac{\mathrm{d}y_F}{\mathrm{d}\eta}\bigg|_{\eta=0^+} = (1 - y_{F0})f(0), \tag{3.28a}$$

$$\frac{\varepsilon}{\Gamma}\frac{\mathrm{d}\theta_g}{\mathrm{d}\eta}\bigg|_{\eta=0^+} = -lf(0) + \varepsilon\frac{J}{a^{1/2}}\frac{\mathrm{d}\theta_l}{\mathrm{d}z}\bigg|_{z=-z_b} - \frac{N_l}{a^{1/2}}\int_{-z_b}^{0}(\theta_s - \theta_l)\,\mathrm{d}z, \tag{3.28b}$$

in which $l \equiv L/(c_p T_\infty \rho_\infty a^{1/2})$. The assumption of a low-volatility liquid is taken into account through $l = O(\Gamma)$. Since the non-dimensional liquid volumetric surface convection heat coefficient satisfies $N_l = O(\Gamma^2)$ and $\Gamma \gg 1$, a quick analysis on the magnitude order of the terms in (3.28*b*) reveals that the main responsible for providing heat to the liquid is the solid matrix (the leading order terms are the first and last terms on the right-hand side of (3.28*b*)). This feature exhibits that the inclusion of a porous matrix into the system leads to an enhancement on the vaporization rate.

The non-dimensional vaporization rate is related with $f(0)$ through

$$-a^{1/2}f(0) = \dot{m}. \tag{3.29}$$

4. Gas–solid region

Above the liquid interface, $\eta > 0$, a gas flow is considered. The analysis performed in the gas–solid region is similar to a previous work (Kokubun & Fachini 2011).

Far from the interface, the only velocity contribution is due to the injected hot gas, but at the gas–liquid interface is due to the plane-normal, low-rate vaporization. Two zones must be separately analysed: an outer zone, related to the solid phase thermal diffusivity, and an inner zone, related to the gas phase thermal diffusivity. In the outer zone, gas and solid are in thermal equilibrium due to the high value of the interphase heat transfer, and macroscopic viscous effects due to gas–liquid interaction are not observed, only the viscous effects due to the porous–fluid interaction are present. Owing to the thermal equilibrium, a one-equation modelling for energy conservation is used. In the inner zone, of the order of Γ^{-1}, the thermal equilibrium is no longer satisfied, and macroscopic viscous effects become relevant. In this zone, a two-equation modelling for the energy conservation is required, in order to account for the thermal non-equilibrium.

Solutions for both regions are obtained by utilizing the perturbation method (Van Dyke 1964; Kevorkian & Cole 1981; Nayfeh 1981), and imposing the matching between inner zone and outer zone profiles.

4.1. *Outer zone*

In a region of the order of unity above the gas–liquid interface, momentum and temperature profiles are obtained from (3.17) to (3.21). Summing (3.20) and (3.21) and since thermal equilibrium is observed in the outer zone, substituting $\theta_s = \theta_g = \theta$, a single equation for the energy conservation is obtained

$$\Gamma^{-1}\theta'' + \gamma\theta'' + f\theta' = 0 \tag{4.1}$$

in which the prime denotes differentiation with respect to η.

Solutions for momentum and temperature are expressed as

$$\left.\begin{aligned} f &= f_{(0)} + \Gamma^{-1}f_{(1)} + O(\Gamma^{-2}), \\ \theta &= \theta_{(0)} + \Gamma^{-1}\theta_{(1)} + O(\Gamma^{-2}). \end{aligned}\right\} \tag{4.2}$$

Substituting the proposed solutions given by (4.2) in (3.18) and (4.1), and collecting terms of similar powers of Γ, the following set of equations are obtained, for momentum and temperature, respectively,

$$f'_{(0)} = 1, \tag{4.3a}$$

$$f_{(0)}f''_{(0)} - (f'_{(0)})^2 - \varepsilon Pr\beta f'_{(1)} = -\varepsilon Pr, \tag{4.3b}$$

$$\gamma\theta''_{(0)} + \eta\theta'_{(0)} = 0, \tag{4.3c}$$

$$\gamma\theta''_{(1)} + f_{(0)}\theta'_{(1)} + \theta''_{(0)} + f_{(1)}\theta'_{(0)} = 0, \tag{4.3d}$$

with boundary conditions far from the interface ($\eta \to \infty$) given by

$$f'_{(0)} - 1 = f'_{(1)} - U_1 = \theta_{(0)} - 1 = \theta_{(1)} = 0, \tag{4.4}$$

and at the interface ($\eta \to 0$)

$$f_{(0)} = f_{(1)} = \theta_{(0)} - \theta_B = \theta_{(1)} - \theta_{s1} = 0. \tag{4.5}$$

It is possible to observe from (4.3*a*) and (4.3*b*) that the flow in the outer zone is predominantly of the Darcy type, with the viscous effects being of higher order. Equation (4.3*c*) exhibits that the heat in the outer zone is transported mainly by conduction (through the solid) and by convection (through the flowing gas). In the outer zone, the low vaporization is not observed, since it is a process confined to the inner zone; due to the low volatility of the liquid, then $f_{(0)}(0) = f_{(1)}(0) = 0$ which means that the vertical component of the velocity v is zero when observed from the outer zone, from the definition of f given in (3.15).

The boundary values of f' for $\eta \to \infty$ are obtained by substituting the expansion of f in (3.17) and applying the limit $\eta \to \infty$, (3.22), obtaining $f' = U_\infty = 1 + \Gamma^{-1}U_1 + O(\Gamma^{-2})$ at $\eta \to \infty$. The leading-order term of such expansion represents the classical Hiemenz flow boundary condition, while the second one indicates the influence of the solid phase on the strain rate (Kokubun & Fachini 2011).

In the outer zone, the main factor responsible for conducting the heat is the solid phase.

Hence, from the outer zone, the observed temperature at the interface is $\theta(0) = \theta_{s0}$. The temperature of the solid phase at the interface, θ_{s0}, is very close to the boiling temperature of the liquid, θ_B. This consideration is taken into account through the boundary condition $\theta(0) = \theta_{s0} = \theta_B + \Gamma^{-1}\theta_{s1} + O(\Gamma^{-1})$, observed from the outer zone. Hence, the temperature θ_{s1} is the deviation of the solid phase temperature at the interface from the boiling temperature of the liquid.

Solving (4.3*a*)–(4.3*d*) with the boundary conditions given by (4.4) and (4.5), momentum and temperature in the outer zone are obtained as

$$f(\eta) = \eta - \Gamma^{-1}\frac{1 - \varepsilon Pr}{\varepsilon\beta Pr}\eta + O(\Gamma^{-2}), \tag{4.6a}$$

$$\theta(\eta) = \theta_B + (1 - \theta_B)\,\mathrm{erf}\left(\frac{\eta}{\sqrt{2\gamma}}\right) - \Gamma^{-1}\left[\frac{(1 - \theta_B)}{2\gamma}\sqrt{\frac{2}{\pi\gamma}}\left(1 + \frac{1 - \varepsilon Pr}{\varepsilon\beta Pr}\gamma\right)\eta \mathrm{e}^{-\eta^2/2\gamma} - \theta_{s1}\left(1 - \mathrm{erf}\left(\frac{\eta}{\sqrt{2\gamma}}\right)\right)\right] + O(\Gamma^{-2}). \tag{4.6b}$$

It is important to emphasize that it is not possible to capture the evaporating effects from the outer zone, hence, justifying the utilization of the boundary conditions $f_{(0)}(0) = f_{(1)}(0) = 0$. This feature is due to the fact that a low-volatility liquid is under consideration, such that the evaporating effects are observed only close to the liquid interface, in the inner zone.

Also, as pointed out previously, it is possible to observe that the flow field in the outer zone is governed by the Darcy equation with linear corrections. Recalling that under a constant pressure gradient, the velocity flow profile is linear, according to the Darcy equation. In this zone, the macroscopic viscous effects (represented by the second and third derivatives in (3.18)) are not observed.

4.2. *Inner zone*

In a length scale of the order of Γ^{-1}, viscous effects due to the gas–liquid interaction, as well as thermal non-equilibrium between gas and solid phase, are observed. In order to capture such variations, a stretching in the spatial coordinate is necessary. This stretching corresponds to a boundary-layer expansion near the gas–liquid interface, and it is given by $\tilde{\eta} = \Gamma\eta$.

As the flow approaches the stagnation point from above, a decrease in the velocity field is observed, and below the stagnation point, the velocity field is a result of the low-rate vaporization of the low-volatility liquid. Hence, in the inner zone, near the interface, a re-scaling in the momentum variable is required and it is given by $\tilde{f} = \Gamma f$, in order to keep it unitary order. It is also observed that in the inner zone the thermal equilibrium is no longer satisfied and, hence, a two-equation modelling for the energy is required.

After performing the spatial coordinate stretching, $\tilde{\eta} = \Gamma\eta$, and the variable re-scaling, $\tilde{f} = \Gamma f$, the equations to be solved are

$$\Gamma Pr\tilde{f}''' + \tilde{f}\tilde{f}'' - (\tilde{f}')^2 - \Gamma\varepsilon\beta Pr\tilde{f}' = -\varepsilon Pr(1+\beta\Gamma), \tag{4.7}$$

$$-\varepsilon\tilde{f}\theta_g' = \Gamma\varepsilon\theta_g'' + \Gamma n_g(\theta_s - \theta_g), \tag{4.8a}$$

$$0 = \Gamma^2(1-\varepsilon)\theta_s'' - \Gamma n_g(\theta_s - \theta_g), \tag{4.8b}$$

in which the prime now denotes differentiation with respect to $\tilde{\eta}$. The solutions are proposed to be expressed as

$$\left.\begin{aligned} \tilde{f} &= \tilde{f}_{(0)} + \Gamma^{-1}\tilde{f}_{(1)} + O(\Gamma^{-2}),\\ \theta_g &= \theta_B + \Gamma^{-1}\theta_{g(1)} + O(\Gamma^{-2}),\\ \theta_s &= \theta_B + \Gamma^{-1}\theta_{s(1)} + O(\Gamma^{-2}). \end{aligned}\right\} \tag{4.9}$$

Substituting the momentum solution in (4.7) and collecting terms of similar powers of Γ, the following equations are found for the first two terms

$$\tilde{f}_{(0)}''' - \varepsilon\beta(\tilde{f}_{(0)}' - 1) = 0, \tag{4.10a}$$

$$Pr\tilde{f}_{(1)}''' + \tilde{f}_{(0)}\tilde{f}_{(0)}'' - (\tilde{f}_{(0)}')^2 - \varepsilon\beta Pr\tilde{f}_{(1)}' = -\varepsilon Pr. \tag{4.10b}$$

One can observe from (4.10*a*) that in its leading order the flow in the inner zone is a balance between the Darcy flow (second term on the left-hand side) and the macroscopic viscous force (first term on the left-hand side), while only in higher order the convection terms appears (second and third terms in the left-hand side of (4.10*b*)). The boundary conditions at $\tilde{\eta} = 0$ are given by

$$\tilde{f}_{(0)} - \tilde{f}_0 = \tilde{f}_{(1)} - \tilde{f}_1 = 0. \tag{4.11}$$

It is relevant to point that $\tilde{f}_0$ accounts for the leading order processes that leads to vaporization, while $\tilde{f}_1$ accounts for the higher order, secondary role, processes. These processes will be recognized when we perform the analysis of the energy conservation at the interface, given by (3.28*b*).

The utilization of the boundary-layer expansion near the interface imposes the condition that the solutions from the inner zone must obey a matching flux condition with the solutions from the outer zone. So, in addition to the boundary conditions presented latter, the solutions of (4.10*a*) and (4.10*b*) must obey

$$\left.\frac{\mathrm{d}\tilde{f}_{(0)}}{\mathrm{d}\tilde{\eta}}\right|_{\tilde{\eta}\to\infty} = \left.\frac{\mathrm{d}f_{(0)}}{\mathrm{d}\eta}\right|_{\eta\to 0}, \quad \left.\frac{\mathrm{d}\tilde{f}_{(1)}}{\mathrm{d}\tilde{\eta}}\right|_{\tilde{\eta}\to\infty} = \left.\frac{\mathrm{d}f_{(1)}}{\mathrm{d}\eta}\right|_{\eta\to 0}. \tag{4.12}$$

It worth mentioning that the conditions established in (4.12) represent the continuity of the flux of momentum between the outer and inner zone. Solving (4.10*a*) and (4.10*b*) with boundary and matching conditions given by (4.11) and (4.12), the momentum in

the inner zone is obtained as

$$\tilde{f}(\tilde{\eta}) = \tilde{f}_0 + \tilde{\eta} + \frac{1}{\sqrt{\varepsilon\beta}}\left(\mathrm{e}^{-\sqrt{\varepsilon\beta}\tilde{\eta}} - 1\right) - \Gamma^{-1}\left\{\tilde{f}_1 + \frac{1}{8\varepsilon\beta\sqrt{\varepsilon\beta}Pr}\left[7(\mathrm{e}^{-\sqrt{\varepsilon\beta}\tilde{\eta}} - 1)\right.\right.$$
$$+ \; 6\sqrt{\varepsilon\beta}\tilde{\eta}\mathrm{e}^{-\sqrt{\varepsilon\beta}\tilde{\eta}} + 8\sqrt{\varepsilon\beta}Pr(1-\varepsilon Pr)\tilde{\eta} + 6(\sqrt{\varepsilon\beta}\tilde{f}_0 + 1)(\mathrm{e}^{-\sqrt{\varepsilon\beta}\tilde{\eta}} - 1)$$
$$+ \; 4\sqrt{\varepsilon\beta}(\sqrt{\varepsilon\beta}\tilde{f}_0 + 1)(\mathrm{e}^{-\sqrt{\varepsilon\beta}\tilde{\eta}} - 1) + 2\varepsilon\beta\tilde{\eta}^2\mathrm{e}^{-\sqrt{\varepsilon\beta}\tilde{\eta}}$$
$$\left.\left. + \; \left(8Pr(1-\varepsilon Pr) - 7 - 2\sqrt{\varepsilon\beta}(3\tilde{f}_0 + 2) - \frac{\tilde{f}_0\varepsilon\beta}{4}\right)\left(\mathrm{e}^{-\sqrt{\varepsilon\beta}\tilde{\eta}} - 1\right)\right]\right\}$$
$$+ O(\Gamma^{-2}). \tag{4.13}$$

The horizontal component of the velocity may be obtained by simply deriving the above expression with respect to $\tilde{\eta}$. At the interface, no horizontal component of the velocity is observed ($\tilde{f}'(\tilde{\eta} = 0) = 0$), since near $\tilde{\eta} = 0$ the velocity field is a result of the liquid vaporization, and this process is characterized by an abrupt phase change, with the expanding gas having only normal component.

Substituting the solutions for the temperatures given in (4.9) in (4.8*a*) and (4.8*b*) and collecting similar powers of Γ, two sets of governing equations are obtained, for the solid and gas phases, respectively,

$$(1-\varepsilon)\theta''_{s(1)} = 0, \tag{4.14a}$$
$$(1-\varepsilon)\theta''_{s(2)} = n_g(\theta_{s(1)} - \theta_{g(1)}), \tag{4.14b}$$

$$\varepsilon\theta''_{g(1)} = -n_g(\theta_{s(1)} - \theta_{g(1)}), \tag{4.15a}$$
$$\varepsilon\theta''_{g(2)} + \varepsilon\tilde{f}_{(0)}\theta'_{g(1)} = -n_g(\theta_{s(2)} - \theta_{g(2)}), \tag{4.15b}$$

in which (4.15*a*) and (4.15*b*) exhibits that the convection heat transport is relevant only in higher order. The boundary conditions at $\tilde{\eta} = 0$ are given by

$$\theta_{s(1)} - \theta_{s1} = \theta_{s(2)} = \theta_{g(1)} = \theta_{g(2)} = 0, \tag{4.16}$$

in which the boundary values for the gas phase temperature are obtained under the consideration of exact equilibrium between gas and liquid phases at the interface. The boundary value for the first correction of the solid temperature, θ_{s1}, is the deviation between gas and solid temperatures at the interface, and as will be seen next, this difference is the main factor responsible for providing the necessary heat to phase change of the liquid.

The matching flux condition (continuity of the heat flux between outer and inner zones) with the outer zone imposes that

$$\left.\frac{\mathrm{d}\theta_{s(1)}}{\mathrm{d}\tilde{\eta}}\right|_{\tilde{\eta}\to\infty} = \left.\frac{\mathrm{d}\theta_{g(1)}}{\mathrm{d}\tilde{\eta}}\right|_{\tilde{\eta}\to\infty} = \left.\frac{\mathrm{d}\theta_{(0)}}{\mathrm{d}\eta}\right|_{\eta\to 0}, \quad \left.\frac{\mathrm{d}\theta_{s(2)}}{\mathrm{d}\tilde{\eta}}\right|_{\tilde{\eta}\to\infty} = \left.\frac{\mathrm{d}\theta_{g(2)}}{\mathrm{d}\tilde{\eta}}\right|_{\tilde{\eta}\to\infty} = \left.\frac{\mathrm{d}\theta_{(1)}}{\mathrm{d}\eta}\right|_{\eta\to 0}. \tag{4.17}$$

Recall that $\theta_{(0)}$ and $\theta_{(1)}$ are the leading order and first correction temperature profiles in the outer zone, respectively. The solutions of (4.14*a*) and (4.14*b*) with boundary and matching conditions given by (4.16) and (4.17) provide the solid phase temperature in

the inner zone as

$$\theta_s(\tilde{\eta}) = \theta_B + \Gamma^{-1}\left[\theta_{s1} + (1-\theta_B)\sqrt{\frac{2}{\pi\gamma}}\tilde{\eta}\right] - \Gamma^{-2}\left[\frac{\theta_{s1}}{\gamma}\left(1-\mathrm{e}^{-\sqrt{n_g/\varepsilon}\tilde{\eta}}\right) + \frac{(1-\theta_B)}{2\gamma}\sqrt{\frac{2}{\pi\gamma}}\left(1+\frac{1-\varepsilon Pr}{\varepsilon\beta Pr}\gamma\right)\tilde{\eta} + \sqrt{\frac{2}{\pi\gamma}}\theta_{s1}\tilde{\eta}\right] + O(\Gamma^{-3}). \tag{4.18}$$

Also, the solutions of (4.15*a*) and (4.15*b*) with boundary and matching conditions given by (4.16) and (4.17) provide the gas phase temperature in the inner zone as

$$\begin{aligned}\theta_g(\tilde{\eta}) = {} & \theta_B + \Gamma^{-1}\left[\theta_{s1}\left(1-\mathrm{e}^{-\sqrt{n_g/\varepsilon}\tilde{\eta}}\right) + (1-\theta_B)\sqrt{\frac{2}{\pi\gamma}}\tilde{\eta}\right] \\ & + \Gamma^{-2}\left[-\frac{\theta_{s1}}{\gamma}\left(1-\mathrm{e}^{-\sqrt{\varepsilon\beta}\tilde{\eta}}\right) - \left(\frac{(1-\theta_B)}{2\gamma}\sqrt{\frac{2}{\pi\gamma}}\left(1+\frac{1-\varepsilon Pr}{\varepsilon\beta Pr}\gamma\right) + \sqrt{\frac{2}{\pi\gamma}}\theta_{s1}\right)\tilde{\eta}\right. \\ & - \frac{1}{\varepsilon\beta}\sqrt{\frac{n_g}{\varepsilon}}\frac{\theta_{s1}}{2\sqrt{n_g/\varepsilon}+\sqrt{\varepsilon\beta}}\left(\mathrm{e}^{-\sqrt{n_g/\varepsilon}\tilde{\eta}}-1\right)\mathrm{e}^{-\sqrt{\varepsilon\beta}\tilde{\eta}} \\ & + \frac{\theta_{s1}}{4}\sqrt{\frac{\varepsilon}{n_g}}\left(\tilde{f}_0 + \sqrt{\frac{n_g}{\varepsilon}}\frac{1}{\gamma} + \frac{1}{\sqrt{\varepsilon\beta}} + \frac{1}{2}\right)\left(\mathrm{e}^{-\sqrt{n_g/\varepsilon}\tilde{\eta}} - \mathrm{e}^{-\sqrt{\varepsilon\beta}\tilde{\eta}}\right) \\ & \left. + \frac{\theta_{s1}}{2}\tilde{\eta}\mathrm{e}^{-\sqrt{n_g/\varepsilon}\tilde{\eta}}\left(\tilde{f}_0 + \sqrt{\frac{n_g}{\varepsilon}}\frac{1}{\gamma} + \frac{1}{\sqrt{\varepsilon\beta}} + \frac{1}{2}\left(1+\sqrt{\frac{n_g}{\varepsilon}}\tilde{\eta}\right)\right)\right] + O(\Gamma^{-3}).\end{aligned} \tag{4.19}$$

In the inner zone, no sink or source energy terms exist. Thus, the deviation between solid and gas temperatures cannot be large. Hence, the choice of the expansions in (4.9) leads to $(\theta_s - \theta_g) = O(\Gamma^{-1})$ in the inner zone (note that the leading order term for both gas and solid is constant, and given by the boiling temperature of the liquid, θ_B).

5. Vapour mass fraction

Above the interface, the flow field is a result of the vapour that arises from the phase change occurring in the boiling zone. The vapour mass fraction is governed by (3.19), with the following boundary conditions

$$y_F(\eta \to \infty) = 0, \quad y_F(\eta = 0) = y_{F0}. \tag{5.1}$$

At the interface, mass conservation must follow

$$\frac{1}{\Gamma}\frac{1}{Le_F}\frac{\mathrm{d}y_F}{\mathrm{d}\eta}\bigg|_{\eta=0^+} = (1-y_{F0})f(0). \tag{5.2}$$

The vapour mass fraction at the interface, y_{F0}, is unknown, and its value will be obtained in § 7 with the aid of (5.2). However, it must be small since the liquid is considered to be low volatility.

Vapour mass transport occurs in two regimes: convection and diffusion. The convection regime (Darcy flow) is imposed by the pressure field on the outer zone and the diffusion regime is imposed by the low vaporization of the liquid in the inner

zone. So, as in the momentum solution, the vapour mass fraction must be solved in the outer zone and in the inner zone. However, an intermediary zone (in which convection and diffusion mass transport balances) is required for the vapour mass fraction solution, as will be seen in the following.

5.1. *Outer zone*

The equation to be solved for the vapour mass fraction is given by

$$\Gamma^{-1}\frac{\mathrm{d}^2 y_F}{\mathrm{d}\eta^2} + Le_F f\frac{\mathrm{d}y_F}{\mathrm{d}\eta} = 0. \tag{5.3}$$

The boundary conditions are

$$y_F(\eta \to \infty) = 0, \quad y_F(\eta \to 0) = 0. \tag{5.4}$$

The condition for $\eta \to 0$ is a consequence of the establishment of the low-vaporization regime. The solution of (5.3) is expressed as

$$y_F = y_{F(0)} + \Gamma^{-1} y_{F(1)} + O(\Gamma^{-2}). \tag{5.5}$$

Substituting (5.5) in (5.3), collecting the terms of similar order of magnitude and solving the resulting set of equations, it is found that in the outer zone, the vapour mass fraction is null

$$y_F(\eta) = 0. \tag{5.6}$$

Since the liquid is considered to be low volatility (by assuming $l = O(\Gamma)$, which exhibits that a high amount of energy is required for a phase change of the liquid to occur), the vaporization regime is low, and as a result, no vapour is observed in the outer zone, as pointed out by (5.6).

In order to observe the vapour mass transport, the analysis must be made in the inner zone. The spatial coordinate must then be stretched as $\tilde{\eta} = \Gamma\eta$, and (5.3) must be analysed in this new coordinate. However, the matching flux procedure is not achievable between outer and inner zone. This demands an intermediary zone between outer and inner zone, to solve the mass transport. In this intermediary zone of the order of $\Gamma^{-1/2}$ there is a balance between convective and diffusive mass transport.

5.2. *Intermediary zone*

The intermediary zone, necessary only for the vapour mass fraction conservation, is analysed by a stretching in the spatial coordinate, given by $\hat{\eta} = \Gamma^{1/2}\eta$, in (5.3). This re-scaling is chosen such that diffusion and convection transport balance. The momentum in this zone is also re-scaled as $\hat{f} = \Gamma^{1/2} f$ (due to the linear decay in the velocity profile, as pointed by (4.6*a*)), and a quick inspection in (3.18) reveals that the momentum in the intermediary zone will be similar to the profile in the outer zone, as given in (4.6*a*), but with the independent variable being $\hat{\eta}$ instead of η.

The vapour mass fraction in the intermediary zone follows then

$$\frac{\mathrm{d}^2 y_F}{\mathrm{d}\hat{\eta}^2} + Le_F\hat{f}\frac{\mathrm{d}y_F}{\mathrm{d}\hat{\eta}} = 0. \tag{5.7}$$

The solution of (5.7) is expressed as

$$y_F = y_{(0)} + O(\Gamma^{-1}). \tag{5.8}$$

Boundary and matching (continuity of the mass flux between the intermediary and outer zones) conditions are given respectively by

$$y_{F(0)}(\hat{\eta} \to 0) = y_{F0}, \quad \left.\frac{\mathrm{d}y_{F(0)}}{\mathrm{d}\hat{\eta}}\right|_{\hat{\eta}\to\infty} = 0. \tag{5.9}$$

Solution of (5.7) with conditions given by (5.9) provides the solution for the vapour mass fraction as

$$y_F(\hat{\eta}) = y_{F0}\ \mathrm{erfc}\left(\hat{\eta}\sqrt{\frac{Le_F}{2}}\right) + O(\Gamma^{-1}). \tag{5.10}$$

The higher order terms are not necessary and will not be obtained.

It is possible to observe from (5.7) that the intermediary zone is the flow region in which the vapour convection and diffusion transport balance.

5.3. *Inner zone*

The vapour mass fraction in the inner zone is obtained from the stretching of the spatial coordinate given by $\tilde{\eta} = \Gamma^{1/2}\hat{\eta}$. Performing this stretching in (5.7), the following equation is obtained

$$\Gamma\frac{\mathrm{d}^2 y_F}{\mathrm{d}\tilde{\eta}^2} + Le_F\tilde{f}\frac{\mathrm{d}y_F}{\mathrm{d}\tilde{\eta}} = 0. \tag{5.11}$$

Such an equation must obey the following boundary and matching conditions, respectively,

$$y_F(0) = y_{F0}, \quad \Gamma\left.\frac{\mathrm{d}y_F}{\mathrm{d}\tilde{\eta}}\right|_{\tilde{\eta}\to\infty} = \Gamma^{1/2}\left.\frac{\mathrm{d}y_F}{\mathrm{d}\hat{\eta}}\right|_{\hat{\eta}\to 0}. \tag{5.12}$$

The solution of (5.11) is expressed as

$$y_F = y_{F(0)} + \Gamma^{-1/2}y_{F(1/2)} + O(\Gamma^{-1}). \tag{5.13}$$

Substituting the solution given by (5.13) in (5.11), the following equations for the first two terms are found

$$\frac{\mathrm{d}^2 y_{F(0)}}{\mathrm{d}\tilde{\eta}^2} = \frac{\mathrm{d}^2 y_{F(1/2)}}{\mathrm{d}\tilde{\eta}^2} = 0. \tag{5.14}$$

Boundary and matching conditions are given, respectively, by

$$y_{F(0)}(0) - y_{F0} = y_{F(1/2)}(0) = 0, \tag{5.15}$$

$$\left.\frac{\mathrm{d}y_{F(0)}}{\mathrm{d}\tilde{\eta}}\right|_{\tilde{\eta}\to\infty} = 0, \quad \left.\frac{\mathrm{d}y_{F(1/2)}}{\mathrm{d}\tilde{\eta}}\right|_{\tilde{\eta}\to\infty} = \left.\frac{\mathrm{d}y_{F(0)}}{\mathrm{d}\hat{\eta}}\right|_{\hat{\eta}\to 0}. \tag{5.16}$$

Solving (5.14) with boundary and matching conditions given by (5.15) and (5.16), the vapour mass fraction in the inner zone is obtained as

$$y_F(\tilde{\eta}) = y_{F0} - \Gamma^{-1/2}y_{F0}\sqrt{\frac{2}{\pi}Le_F}\tilde{\eta} + O(\Gamma^{-1}). \tag{5.17}$$

In the inner zone, the mass diffusion is the dominant process, as pointed out by (5.11) and (5.17).

6. Liquid–solid region

To distinguish the gas–solid region from the liquid–solid region, the spatial variable z is used instead of η. In the region $z < 0$, the solid matrix is filled with the liquid. Far below the interface, liquid and solid matrix are in thermal equilibrium due to the high rate of heat transfer between the phases. In this zone, denoted as the equilibrium zone, a one-equation modelling is enough to describe the temperature profile. The equilibrium zone presents two length scales: one of the order of Γ, and another of the order of unity, as will be shown ahead. The existence of two different zones is a result of the low-vaporization rate.

In a length scale of the order of Γ^{-1} below the interface, the liquid is at an almost constant temperature, its boiling temperature, and all of the heat provided to it in this zone goes to phase change. The solid phase, on the other hand, does not have such physical constraints, and its temperature continues to rise as an effect of the heat flux from the gas–solid region. Under such considerations, a detachment between the temperatures profiles is observed, and a two-equation modelling is required, with the imposition of the matching flux condition with the solution obtained in the equilibrium zone.

6.1. *Equilibrium zone*

In a large region below the interface thermal equilibrium between solid and liquid phases is observed, and a single equation for the energy conservation is required. Summing (3.25) and (3.26) and considering $\theta_s = \theta_l = \theta$, the following equation is obtained

$$\left(\frac{J+\gamma}{M}\right)\frac{\mathrm{d}^2\theta}{\mathrm{d}z^2} - \frac{\mathrm{d}\theta}{\mathrm{d}z} = 0, \tag{6.1}$$

in which $M \equiv \dot{m}(c_l/c_p)$ and $J \equiv \lambda_l/\lambda_s = O(1)$. The boundary condition far below the interface ($z \to -\infty$) is

$$\theta = \theta_{-\infty}, \tag{6.2}$$

and at the liquid surface, $z = 0$,

$$\theta = \theta_B. \tag{6.3}$$

The solution of (6.1) with boundary conditions given by (6.2) and (6.3) provides the temperature in the equilibrium zone

$$\theta(z) = (\theta_B - \theta_{-\infty})\mathrm{e}^{zM/(J+\gamma)} + \theta_{-\infty}. \tag{6.4}$$

It is recalled that M is related with the vaporization rate through $M = -a^{1/2}(c_l/c_p)f(0)$ (from the definition of M and (3.29)), and since the vaporization is low (low-volatility liquid), it is pointed that $M = O(\Gamma^{-1})$. With this in mind, it is possible to observe that (6.4) presents a variation of the order of unity in a region of the order of Γ. In order to analyse the zone of the order of unity, a Taylor expansion for small values of $zM/(J+\gamma)$ is performed, and the obtained expression is given by

$$\theta(z) = \theta_B + (\theta_B - \theta_{-\infty})\left\{\Gamma^{-1}\frac{M_0}{J+\gamma}z + \Gamma^{-2}\left[\frac{M_1}{J+\gamma}z + \left(\frac{M_0}{J+\gamma}\right)^2 z^2\right] + O(\Gamma^{-3})\right\}, \tag{6.5}$$

in the above, $M = \Gamma^{-1}M_0 + \Gamma^{-2}M_1$, in which $M_0 = -a^{1/2}(c_l/c_p)\tilde{f}_0$ and $M_1 = -a^{1/2}(c_l/c_p)\tilde{f}_1$.

6.2. *Boiling zone*

In a characteristic length scale of the order of Γ^{-1} below the interface, thermal non-equilibrium is observed. In order to capture such variations in the liquid and solid phases temperature, a stretching in the spatial coordinate is necessary and given by $\tilde{z} = \Gamma z$. This stretching is performed in (3.25) and (3.26), obtaining

$$\Gamma^2 \varepsilon J \frac{\mathrm{d}^2\theta_l}{\mathrm{d}\tilde{z}^2} - \Gamma \varepsilon M \frac{\mathrm{d}\theta_l}{\mathrm{d}\tilde{z}} = -\Gamma^2 n_l(\theta_s - \theta_l), \tag{6.6}$$

$$\Gamma^2(1-\varepsilon)\frac{\mathrm{d}^2\theta_s}{\mathrm{d}\tilde{z}^2} = \Gamma^2 n_l(\theta_s - \theta_l). \tag{6.7}$$

The solutions for the temperatures are expressed as

$$\left.\begin{aligned} \theta_l &= \theta_B + \Gamma^{-2}\theta_{l(2)} + O(\Gamma^{-3}), \\ \theta_s &= \theta_B + \Gamma^{-1}\theta_{s(1)} + \Gamma^{-2}\theta_{s(2)} + O(\Gamma^{-3}). \end{aligned}\right\} \tag{6.8}$$

In the boiling zone, almost all heat provided to the liquid goes to phase change and, hence, its temperature is considered a constant, θ_B, in its leading order. The term of the order of Γ^{-1} of the liquid is null because there are no physical processes influencing on that order (recalling that no source or sink terms exist in the boiling zone and that the temperature at the interface is exactly the boiling temperature). However, the heat flux matching condition with the equilibrium zone must be obeyed. The matching flux condition imposes that $\Gamma \mathrm{d}\theta_{s,g}/\mathrm{d}\tilde{z}|_{\tilde{z}\to-\infty} = \mathrm{d}\theta/\mathrm{d}z|_{z\to 0}$, which, according to (6.5), is of the order of Γ^{-1}.

Hence, the term of the order of Γ^{-2} is non-zero, in order to match the solution with the unitary order equilibrium zone, given by (6.5).

Substituting (6.8) in (6.6) and (6.7) and collecting similar powers of Γ, the following set of equations is found

$$\varepsilon J \frac{\mathrm{d}^2\theta_{l(2)}}{\mathrm{d}\tilde{z}^2} = -n_l(\theta_{s(2)} - \theta_{l(2)}), \tag{6.9a}$$

$$(1-\varepsilon)\frac{\mathrm{d}^2\theta_{s(1)}}{\mathrm{d}\tilde{z}^2} = n_l\theta_{s(1)}, \tag{6.9b}$$

$$(1-\varepsilon)\frac{\mathrm{d}^2\theta_{s(2)}}{\mathrm{d}\tilde{z}^2} = n_l(\theta_{s(2)} - \theta_{l(2)}). \tag{6.9c}$$

The boundary conditions at $\tilde{z} = 0$ are given by

$$\theta_{s(1)} - \theta_{s1} = \theta_{s(2)} = \theta_{l(2)} = 0. \tag{6.10}$$

Also, the matching flux condition (the continuity of the heat flux between the equilibrium and the boiling zone in the liquid–solid region) must be satisfied, then

$$\left.\frac{\mathrm{d}\theta_{s(1)}}{\mathrm{d}\tilde{z}}\right|_{\tilde{z}\to-\infty} = 0, \quad \left.\frac{\mathrm{d}\theta_{s(2)}}{\mathrm{d}\tilde{z}}\right|_{\tilde{z}\to-\infty} = \left.\frac{\mathrm{d}\theta_{l(2)}}{\mathrm{d}\tilde{z}}\right|_{\tilde{z}\to-\infty} = \left.\frac{\mathrm{d}\theta_{(1)}}{\mathrm{d}z}\right|_{z\to 0} = M_0\left(\frac{\theta_B - \theta_{-\infty}}{J+\gamma}\right) \tag{6.11}$$

in which the variable z and the first correct value of the temperature $\theta_{(1)}$ are values from the unitary order equilibrium zone, given by (6.5).

Solving (6.9*a*)–(6.9*c*) with boundary and matching conditions given by (6.10) and (6.11), the temperature solutions for the boiling zone are obtained as

$$\theta_l(\tilde{z}) = \theta_B + \Gamma^{-2}M_0\left(\frac{\theta_B - \theta_{-\infty}}{J+\gamma}\right)\tilde{z} + O(\Gamma^{-3}), \tag{6.12a}$$

$$\theta_s(\tilde{z}) = \theta_B + \Gamma^{-1}\theta_{s1}\mathrm{e}^{\sqrt{n_l/(1-\varepsilon)}\tilde{z}} + \Gamma^{-2}M_0\left(\frac{\theta_B - \theta_{-\infty}}{J+\gamma}\right)\tilde{z} + O(\Gamma^{-3}). \quad (6.12b)$$

It is possible to see from (6.12*a*) and (6.12*b*) that the difference from the solid phase temperature and the liquid phase temperature in the boiling zone is of the order of Γ^{-1}.

7. Determination of the unknowns: y_{F0}, θ_{s1}, $\tilde{f}_0$ and $\tilde{f}_1$

If (5.2) is expanded, mass conservation at the interface will be given by

$$\left.\frac{\mathrm{d}\tilde{y}_F}{\mathrm{d}\tilde{\eta}}\right|_{\tilde{\eta}=0^+} = \Gamma^{-1}(1-y_{F0})(\tilde{f}_0 + \Gamma^{-1}\tilde{f}_1). \quad (7.1)$$

From (5.17), the derivative of $\tilde{y}_F$ at $\tilde{\eta} = 0^+$ is determined, and by collecting the leading order terms in (7.1), the vapour mass fraction at the interface is obtained as

$$y_{F0} = \frac{\tilde{f}_0}{\tilde{f}_0 - \Gamma^{1/2}\sqrt{2Le_F/\pi}}. \quad (7.2)$$

Since $\tilde{f}_0 = \Gamma f_0 = O(1)$, it is possible to observe that $y_{F0} = O(\Gamma^{-1/2})$. This is a consequence of the existence of the intermediary zone, which is of the order of $\Gamma^{-1/2}$.

The low-volatility feature of the liquid is considered through high latent heat l and mathematically it means $l = \Gamma\tilde{l}$, in which $\tilde{l}$ is of unitary order. Performing the appropriate changes in (3.28*b*), the energy conservation at the interface is given by

$$\varepsilon\left.\frac{\mathrm{d}\theta_g}{\mathrm{d}\tilde{\eta}}\right|_{\tilde{\eta}=0^+} = -\Gamma\tilde{l}f(0) + \Gamma\varepsilon\frac{J}{a^{1/2}}\left.\frac{\mathrm{d}\theta_l}{\mathrm{d}\tilde{z}}\right|_{\tilde{z}\to-\infty} - \Gamma\frac{n_l}{a^{1/2}}\int_{-\infty}^{0}(\theta_s - \theta_l)\,\mathrm{d}\tilde{z}, \quad (7.3)$$

and it must be noted that $\Gamma f(0) = \tilde{f}_0 + \Gamma^{-1}\tilde{f}_1$.

Expanding (7.3) and collecting the leading order terms (first and third terms on the left-hand side), the leading order velocity at the interface is found as

$$\tilde{f}_0 = -\sqrt{\frac{n_l}{a}}\frac{\theta_{s1}}{\tilde{l}}(1-\varepsilon)^{1/2}. \quad (7.4)$$

The higher order velocity at the interface is obtained by collecting the higher order terms in (7.3)

$$\tilde{f}_1 = -\frac{1}{\tilde{l}}\left[(1-\theta_B)\sqrt{\frac{2}{\pi\gamma}} + \theta_{s1}\sqrt{\frac{n_g}{\varepsilon}}\right] + \frac{J}{J+\gamma}\frac{(\theta_B - \theta_{-\infty})}{\tilde{l}}\frac{M_0}{a^{1/2}}. \quad (7.5)$$

The velocity at the interface is directly related to the vaporization rate through (3.29). Re-scaling (3.29), the vaporization rate is obtained as

$$\Gamma\dot{m} \equiv \dot{\tilde{m}} = \sqrt{n_l}\frac{\theta_{s1}}{\tilde{l}}(1-\varepsilon)^{1/2} + \Gamma^{-1}\left\{\frac{a^{1/2}}{\tilde{l}}\left[(1-\theta_B)\sqrt{\frac{2}{\pi\gamma}} + \theta_{s1}\sqrt{\frac{n_g}{\varepsilon}}\right]\right.$$
$$\left. - \sqrt{n_l}\frac{c_l}{c_p}\left(\frac{J}{J+\gamma}\right)\frac{(\theta_B - \theta_{-\infty})}{\tilde{l}^2}\theta_{s1}(1-\varepsilon)^{1/2}\right\} + O(\Gamma^{-2}). \quad (7.6)$$

The leading order term in (7.6) (first term on the right-hand side) arises from the heat exchange between solid and liquid phases in the boiling zone. Hence, the result

obtained by (7.6) exhibits that the main responsible for providing the heat necessary for the phase change of the liquid is the solid phase, that conductively carries heat from the inner zone to the boiling zone. The gas–liquid heat exchange at the interface has a minor role in such process (of the order of Γ^{-1}), accounted for by the higher order term in (7.6).

The continuity of the solid phase heat flux at the gas–liquid interface requires that

$$\Gamma \left.\frac{\mathrm{d}\theta_s}{\mathrm{d}\tilde{\eta}}\right|_{\tilde{\eta}\to 0^+} = \Gamma \left.\frac{\mathrm{d}\theta_s}{\mathrm{d}\tilde{z}}\right|_{\tilde{z}\to 0^-}. \tag{7.7}$$

If the above expression is expanded and terms with similar order of magnitude are collected, the correction of the solid phase temperature at the interface is obtained as

$$\theta_{s1} = (1-\theta_B)\sqrt{\frac{2\varepsilon}{\pi n_l}}. \tag{7.8}$$

Hence, the solid phase temperature at the interface is given by

$$\theta_s(0) = \theta_B + \Gamma^{-1}(1-\theta_B)\sqrt{\frac{2\varepsilon}{\pi n_l}}. \tag{7.9}$$

From (7.9) it is possible to observe that higher porosity values lead to higher values on the solid phase temperature at the interface, as a result of the increase in the density of the heat flux in the solid phase.

It must be pointed that in order that both sides of (7.7) have the same order of magnitude (otherwise, the solid heat flux continuity would not be obeyed), $(1-\theta_B)$ must be of the order of unity (since $\theta_{s1} = O(1)$, as a result of the matching condition with the outer zone). The temperatures were normalized according to the injection temperature of the hot gas. With this in mind, the restriction that appears reveals that, in order that a solution of the problem is achieved (or, in other words, the vaporization process occurs), the injected gas must be at a temperature higher than the boiling temperature of the liquid, enough for $(1-\theta_B) = O(1)$. This feature is due to the low volatility of the liquid, which demands a high heat flux in order to go through phase change.

In the absence of the porous medium, the vaporization would be much less efficient (of the order of Γ^{-2}, since it would be led by the low-efficiency process of heat exchange between gas and liquid at the interface). However, even with the solid matrix conductively transporting heat, and transferring it, to the liquid reservoir, the vaporization process is still low (of the order of Γ^{-1}).

8. Results and discussion

In order to obtain numerical values for the unknowns, the following values for the parameters are used

$$a = \tilde{l} = n_l = n_g = 1.0, \tag{8.1}$$

$$\varepsilon = 0.3, \quad \Gamma \equiv \bar{\lambda}_s/\bar{\lambda}_g = 60.0, \quad J \equiv \bar{\lambda}_l/\bar{\lambda}_s = 1.0, \tag{8.2}$$

$$\theta_B = 0.2, \quad \theta_{-\infty} = 0.1, \quad Pr = Le_F = 1.0, \quad c_l/c_p = 2.0. \tag{8.3}$$

The injection temperature is considered to be five times the value of the boiling temperature of the liquid, and the reservoir is assumed to be at half of the liquid boiling temperature (recalling that the temperatures were made non-dimensional with

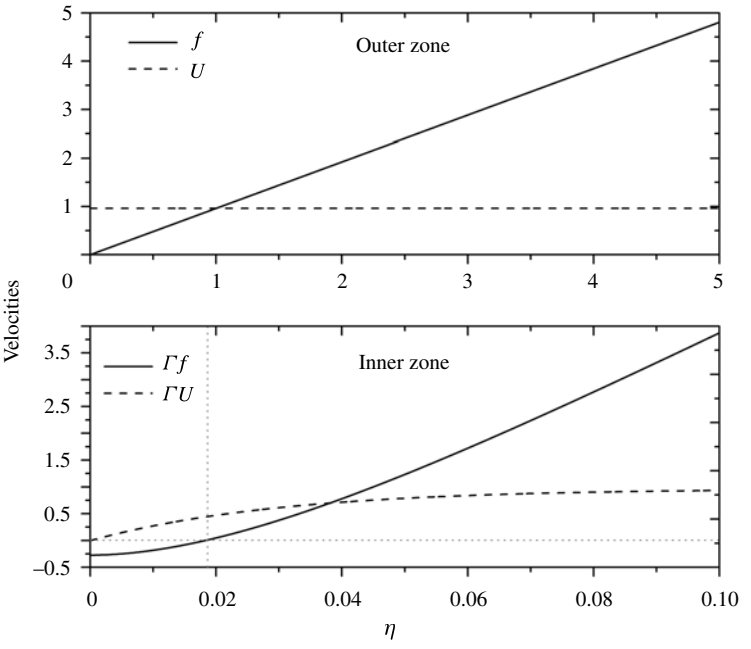

FIGURE 2. Vertical (f) and horizontal ($U = \mathrm{d}f/\mathrm{d}\eta$) velocities.

respect to the injection temperature). The porosity is chosen according to average values in petroleum wells, and the ratio $c_l/c_p = 2.0$ is chosen according to values of specific heat for petroleum and air.

For those parameters, the following values are found:

$$\tilde{f}_0 \simeq -0.2925, \quad \tilde{f}_1 \simeq -1.0386, \quad \theta_{s1} \simeq 0.3496, \quad y_{F0} \simeq 0.0452. \tag{8.4}$$

8.1. *Momentum*

The velocity field of the flow in most of the domain is dominated by the Darcy regime, in which the pressure gradient pushes the injected hot gas onto the liquid surface. Only close to the gas–liquid interface it is possible to observe the small contribution to the velocity field due to the vapour transport, and the viscous terms, which establish the macroscopic and porous-level boundary layers, influence on the flow.

These features may be observed in figure 2, in which the vertical and the horizontal component of the momentum are plotted. The stagnation plane is located approximately in the region in which $\tilde{f}(\tilde{\eta}_{st}) = 0$, at $\eta_{st} = \Gamma^{-1}\tilde{\eta}_{st} \simeq 0.0183$, very close to the liquid interface.

8.2. *Temperature: gas–solid region*

The gas and the solid matrix are assumed to be at equilibrium in the injection condition. The gas–solid system loses heat to the liquid reservoir below the gas–liquid interface.

Owing to the high rates of interphase heat transfer, accounted through the consideration that $N_g = O(\Gamma)$, between gas and solid phases, thermal equilibrium is observed in the outer zone, in which heat is transported conductively (through the solid phase) and convectively (through the gas phase), as pointed by (4.1). As the

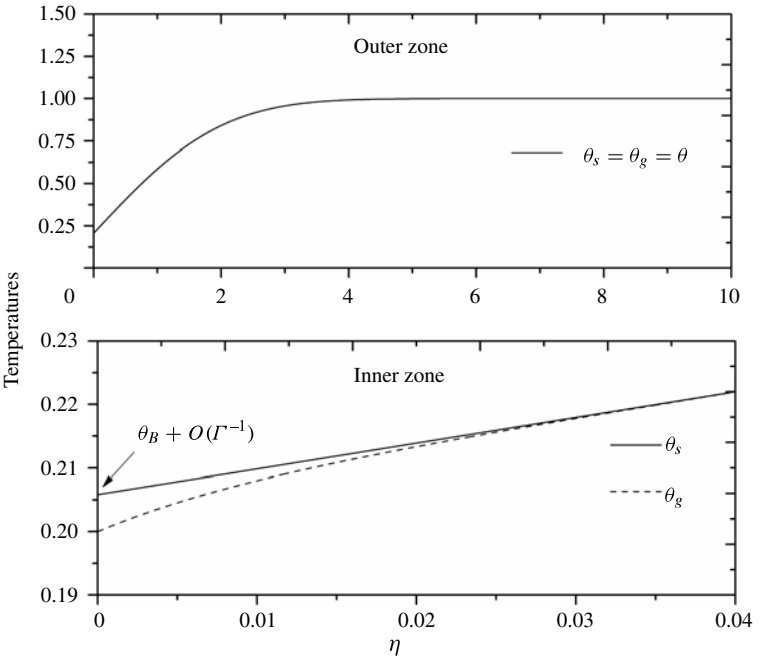

FIGURE 3. Thermal equilibrium in the outer zone and non-equilibrium in the inner zone.

flowing gas approaches the interface from above, a detachment between temperature profiles is observed, as local thermal non-equilibrium is observed in the region of the order of Γ^{-1} (inner zone). In the inner zone, the heat is conducted mainly through the solid phase (higher thermal conductivity), and at the interface, vapour and liquid are at equilibrium at the liquid boiling temperature θ_B, while the solid phase is at a temperature slightly higher (boiling temperature plus a correction of the order of Γ^{-1}, as given by (7.9)).

The quantitative behaviour of the temperatures in the gas–solid region is presented in figure 3.

8.3. *Temperature: liquid–solid region*

Far below the interface, the liquid reservoir is at equilibrium with the solid matrix and both are initially at half the liquid boiling temperature. As a result of the heat flux from the injected gas (and the conduction through the solid matrix), the liquid–solid system increases its temperature. Owing to the high rates of liquid–solid heat transfer, accounted for through the consideration that $N_l = O(\Gamma^2)$, thermal equilibrium between phases is observed.

The low-volatility feature of the liquid (high latent heat of vaporization, accounted for through $l = O(\Gamma)$) is responsible for the establishment of a low-vaporization regime. This feature also expands the thermal equilibrium zone to a region of the order of Γ. Hence, two length scales in the equilibrium zone are observed, one of the order of Γ and the other of the order of unity, as pointed out by (6.5). Only in a region of the order of Γ^{-1} below the interface the thermal non-equilibrium between liquid and solid phases is observed. In this region, the boiling zone, the liquid is at an almost constant temperature, its boiling temperature, and almost all heat provided to it goes to

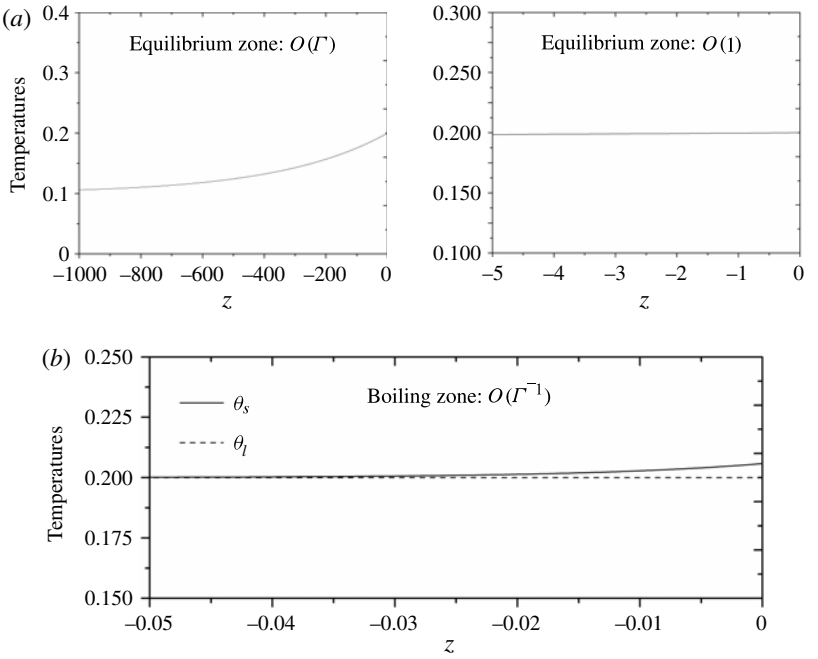

FIGURE 4. Two scales in the equilibrium zone (*a*) and boiling zone (*b*).

phase change. A minor amount of heat is transported into the equilibrium zone, which has a reach of the order of Γ, in order to increase the reservoir temperature (liquid + solid matrix, at equilibrium).

These quantitative features of the temperature profiles in both zones are presented in figure 4.

8.4. *Effects of the strain rate and of the porosity*

The effects of the strain rate a and of the porosity ε in the vaporization rate are presented in figure 5.

If the strain rate is increased, the leading order vaporization rate does not alter, as pointed out by (7.6). A variation in the strain rate from 0.3 to 3.0 leads to an increase in the vaporization rate from 0.295 to 0.300, as exhibited in figure 5. An increase in the strain rate means an approach of the impinging flow against the liquid surface (or, similarly, an increase on the horizontal component of the injection velocity). Such situation would lead the velocity field closer to the interface. However, since the leading order vaporization rate is determined only by the heat exchange between solid and liquid phases in the boiling zone (as pointed by (7.3) and (7.6)), this increase in the strain rate does not affect the vaporization rate in its leading order.

An increase in the solid phase temperature at the interface leads to an increase in the vaporization rate. The solid phase temperature at the interface, $\theta_{s0} = \theta_B + \Gamma^{-1}\theta_{s1}$, is directly proportional to the square root of medium porosity, $\sqrt{\varepsilon}$, as pointed by (7.9). However, as exhibited by the leading order term of (7.6), the vaporization rate is also proportional to $\sqrt{(1-\varepsilon)}$, which is the square root of the volume occupied by the solid phase. Combining both contributions, it is observed that the vaporization rate is proportional to $\sqrt{\varepsilon(1-\varepsilon)}$, as can be seen in figure 5. Two other conclusions can be

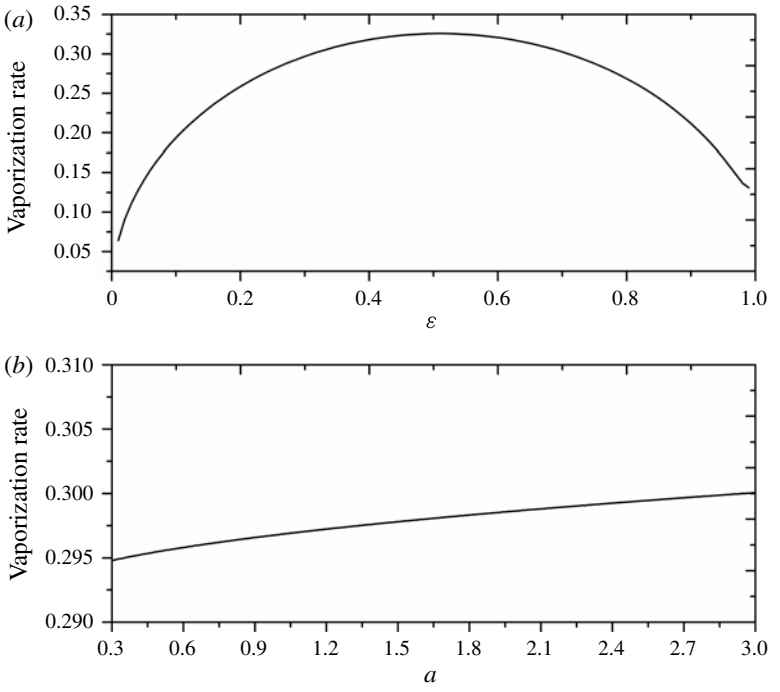

FIGURE 5. Vaporization rate dependence on porosity (a, with $a = 1.0$) and on strain rate (b, with $\varepsilon = 0.3$).

drawn: in the first approximation, the vaporization rate is unexpectedly independent on the liquid heat transfer parameter n_l and expectedly proportional to the reciprocal latent heat l.

In the two limits (high porosity, $\varepsilon \sim 1$, and low porosity, $\varepsilon \ll 1$), the vaporization is low. This effect may be explained in the following. In the higher porosity regime, $\varepsilon \sim 1$; if one lowers the medium porosity, the contact area between liquid and solid is increased, which increases the heat exchange between solid and liquid. This has the effect of enhancing the vaporization rate. On the other hand, if the porosity is lowered enough, the space occupied by the liquid diminishes, which in turn has the consequence of lowering the vaporization rate. Owing to these two processes, the vaporization rate has a minimum in both extreme values of the medium porosity, and a maximum observed in $\varepsilon = 0.5$.

9. Conclusions

By performing an asymptotic analysis and utilizing order of magnitude arguments, the main physical processes of a stationary Hiemenz flow in a low-porosity medium with phase change of a low-volatility liquid have been described analytically. The effects of the strain rate and of the porosity in the vaporization rate have also been examined.

The problem is analysed under the distinguished limit $N_g = O(\Gamma)$, $N_l = O(\Gamma^2)$ and $\kappa = O(\Gamma^{-2})$, in which $\Gamma \equiv \lambda_s/\lambda_g \gg 1$. The first two conditions characterize intense interphase heat transfer (liquid–solid and gas–solid, respectively), while the third may characterize a low-porosity medium (recalling that the parameter $\kappa \equiv aK/ls_s^2$, a

modified Darcy number, relates geometric properties of the solid with thermo-physical properties of solid and gas phases).

The system is considered infinite to both streams, with the gas–liquid interface dividing the domain. In the upper stream, a hot gas is injected. Owing to the high rates of interphase heat transfer, the gas–solid system is at equilibrium in most of the domain. Close to the interface, local thermal non-equilibrium is observed, and the two-equation model is employed.

Below the interface, the solid matrix is filled by the low-volatility liquid. The heat is provided to the liquid reservoir by the injection of the hot stream of gas. However, it is the solid matrix that conductively transports heat to the liquid–solid region. Once in the liquid–solid region, the heat exchange between solid and liquid phases in the boiling zone (a region of the order of $\Gamma^{-1} \ll 1$ close to the liquid interface) supplies the necessary heat in order to phase change the liquid. Since almost all heat is delivered to the phase change, a small amount of heat (of the order of Γ^{-1}) is transported to the reservoir in order to increase its temperature. The gas–liquid heat transfer at the interface has a minor role in the vaporization process, and its effect is accounted for through a correction in the vaporization rate, given by $\tilde{f}_1$. The obtained results quantify the importance of the addition of the porous medium in the enhancement of the evaporation process.

The results also point that in order to sustain the vaporization regime of the low-volatility liquid, the injection temperature must be higher than the liquid boiling temperature, enough for $(1 - \theta_B) = O(1)$. This constraint, which arises as a condition for the continuity of the heat flux at the interface, is a result of the low-volatility feature of the liquid, which demands a high heat flux in order to go through phase change. It is relevant to point that the prediction of high injection temperatures is in accordance with the steam injection and *in situ* combustion processes of thermal oil recovery.

Acknowledgements

This work was partially supported by Coordenação de Aperfeiçoamento de Pessoal de Nível Superior (CAPES), Conselho Nacional de Desenvolvimento Científico e Tecnológico-CNPq under the grant 303046/2010-4 and Fundação de Amparo à Pesquisa do Estado de São Paulo (FAPESP) under the grant 2010/18077-1.

REFERENCES

ALKAM, M. K. & AL-NIMR, M. A. 1999 Improving the performance of double-pipe heat exchangers by using porous substrates. *Intl J. Heat Mass Transfer* **42**, 3609–3618.

ARNOLD, F. C. 1989 A physical model for two-phase flow in steam injection wells. *J. Petrol. Sci. Engng* **3**, 173–183.

BERGINS, C., CRONE, S. & STRAUSS, K. 2005 Multiphase flow in porous media with phase change. Part II. Analytical solutions and experimental verification for constant pressure steam injection. *Transp. Porous Med.* **60**, 275–300.

CASTANIER, L. M. & BRIGHAM, W. E. 2003 Upgrading of crude oil via in situ combustion. *J. Petrol. Sci. Engng* **39**, 125–136.

DAURELLE, J. V., TOPIN, F. & OCCELLI, R. 1998 Modeling of coupled heat and mass transfers with phase change in a porous medium: application to superheated steam drying. *Numer. Heat Transfer (Part* A) **33**, 39–63.

DUVAL, F., FICHOT, F. & QUINTARD, M. 2004 A local thermal non-equilibrium model for two-phase flows with phase-change in porous media. *Intl J. Heat Mass Transfer* **47**, 613–639.

DYGA, R. & PLACZEK, M. 2010 Efficiency of heat transfer in heat exchangers with wire mesh packing. *Intl J. Heat Mass Transfer* **53**, 5499–5508.

FARCAS, A. & WOODS, A. W. 2007 On the extraction of gas from multilayered rock. *J. Fluid Mech.* **581**, 79–95.

FURBERG, R., PALM, B., LI, S., TOPRAK, M. & MUHAMMED, M. 2009 The use of a nano- and microporous surface layer to enhance boiling in a plate heat exchanger. *J. Heat Transfer* **131**, 101010.

IL'ICHEV, A. T., TSYPKIN, G. G., PRITCHARD, D. & RICHARDSON, C. N. 2008 Instability of the salinity profile during the evaporation of saline groundwater. *J. Fluid Mech.* **614**, 87–104.

JABBOUR, C., QUINTARD, M., BERTIN, H. & ROBIN, M. 1996 Oil recovery by steam injection: three-phase flow effects. *J. Petrol. Sci. Engng* **16**, 109–130.

KEVORKIAN, J. & COLE, J. D. 1981 *Perturbation Methods in Applied Mathematics* (ed. F. John, J. E. Mardsen & L. Sirovich), pp. 370–387. Springer.

KOKUBUN, M. A. E. & FACHINI, F. F. 2011 An analytical approach for a Hiemenz flow in a porous medium with heat exchange. *Intl J. Heat Mass Transfer* **54**, 3613–3621.

KONSTATINOU, N. D., STUBOS, A. K., STATHARAS, J. C., KANELLOPOULOS, N. K. & PAPAIOANNOU, A. C. 1997 Enhanced boiling heat transfer in porous layers with application to electronic component cooling. *J. Enhanced Heat Transfer* **4**, 175–186.

LEHMANN, P., ASSOULINE, S. & OR, D. 2008 Characteristic length scales affecting evaporative drying of porous media. *Phys. Rev.* E **77**, 056309.

LITER, S. G. & KAVIANY, M. 2001 Pool-boiling CHF enhancement by modulated porous-layer coating: theory and experiment. *Intl J. Heat Mass Transfer* **44**, 4287–4311.

NAYFEH, A. H. 1981 *Introduction to Perturbation Techniques*, pp. 257–303. John Wiley & Sons.

PEREIRA, F. M., OLIVEIRA, A. A. M. & FACHINI, F. F. 2009 Asymptotic analysis of stationary adiabatic premixed flames in porous inert media. *Combust. Flame* **156**, 152–165.

PEREIRA, F. M., OLIVEIRA, A. A. M. & FACHINI, F. F. 2010 Theoretical analysis of ultra-lean premixed flames in porous inert media. *J. Fluid Mech.* **657**, 285–307.

PRATS, M. 2003 Effect of steam injection into two nearby layers. *J. Petrol. Sci. Engng* **39**, 117–124.

RAMESH, P. S. & TORRANCE, K. E. 1993 Boiling in a porous layer heated from below: effects of natural convection and a moving liquid/two-phase interface. *J. Fluid Mech.* **257**, 289–309.

REES, D. A. S., BASSOM, A. P. & SIDDHESHWAR, P. G. 2008 Local thermal non-equilibrium effects arising from the injection of a hot fluid into a porous medium. *J. Fluid Mech.* **594**, 379–398.

SCHILICHTING, H. 1968 *Boundary-layer Theory*, pp. 81–86. McGraw-Hill.

TSYPKIN, G. G. & WOODS, A. W. 2004 Vapour extraction from a water-saturated geothermal reservoir. *J. Fluid Mech.* **506**, 315–330.

TSYPKIN, G. G. & WOODS, A. W. 2005 Precipitate formation in a porous rock through evaporation of saline water. *J. Fluid Mech.* **537**, 35–53.

VAN DYKE, M. 1964 *Perturbation Methods in Fluid Mechanics* (ed. F. N. Frenkel & G. Temple), pp. 77–97. Academic Press.

WOODS, A. W. 1999 Liquid and vapour flow in superheated rock. *Annu. Rev. Fluid Mech.* **31**, 171–199.

WOODS, A. W. & FITZGERALD, S. D. 1993 The vaporization of a liquid front moving through a hot porous rock. *J. Fluid Mech.* **251**, 563–579.

YANG, Y. T. & HWANG, M. L. 2009 Numerical simulation of turbulent fluid flow and heat transfer characteristics in heat exchangers fitted with porous media. *Intl J. Heat Mass Transfer* **52**, 2956–2965.

YORTSOS, Y. C. & STUBOS, A. K. 2001 Phase change in porous media. *Curr. Opin. Colloid Interface Sci.* **6**, 208–216.

ZHAO, T. S. 1999 Coupled heat and mass transfer of a stagnation point flow in a heated porous bed with liquid film evaporation. *Intl J. Heat Mass Transfer* **42**, 861–872.